TOPICAL REVIEW

Advances in volumetric bioprinting

Biofabrication

TOPICAL REVIEW

Advances in volumetric bioprinting

Sibo Jing[1,5], Liming Lian[2,5], Yingying Hou[1,5], Zeqing Li[1], Zihao Zheng[1], Gang Li[3], Guosheng Tang[4], Guoxi Xie[1] and Maobin Xie[1,*]

[1] The Sixth Affiliated Hospital of Guangzhou Medical University, Qingyuan People's Hospital, Guangzhou Municipal and Guangdong Provincial Key Laboratory of Protein Modification and Degradation, School of Biomedical Engineering, Guangzhou Medical University, Guangzhou 511436, People's Republic of China
[2] Wallace H. Coulter Department of Biomedical Engineering, Georgia Institute of Technology, Atlanta, GA 30332, United States of America
[3] National Engineering Laboratory for Modern Silk, College of Textile and Clothing Engineering, Soochow University, Suzhou 215123, People's Republic of China
[4] Guangzhou Municipal and Guangdong Provincial Key Laboratory of Molecular Target & Clinical Pharmacology, The NMPA and State Key Laboratory of Respiratory Disease, School of Pharmaceutical Sciences and the Fifth Affiliated Hospital, Guangzhou Medical University, Guangzhou 511436, People's Republic of China
[5] These authors contributed equally to this work.
[*] Authors to whom any correspondence should be addressed.

E-mail: maobinxie@gzhmu.edu.cn

Keywords: volumetric bioprinting, biofabrication, (bio)ink, biomedical application

RECEIVED
15 June 2023

REVISED
16 October 2023

ACCEPTED FOR PUBLICATION
3 November 2023

PUBLISHED
28 November 2023

Abstract

The three-dimensional (3D) bioprinting technologies are suitable for biomedical applications owing to their ability to manufacture complex and high-precision tissue constructs. However, the slow printing speed of current layer-by-layer (bio)printing modality is the major limitation in biofabrication field. To overcome this issue, volumetric bioprinting (VBP) is developed. VBP changes the layer-wise operation of conventional devices, permitting the creation of geometrically complex, centimeter-scale constructs in tens of seconds. VBP is the next step onward from sequential biofabrication methods, opening new avenues for fast additive manufacturing in the fields of tissue engineering, regenerative medicine, personalized drug testing, and soft robotics, etc. Therefore, this review introduces the printing principles and hardware designs of VBP-based techniques; then focuses on the recent advances in VBP-based (bio)inks and their biomedical applications. Lastly, the current limitations of VBP are discussed together with future direction of research.

1. Introduction

Bioprinting is an evolving research field, which attracts attentions from tissue engineering, regenerative medicine, personalized drug testing etc [1–3]. Normally, three-dimensional printing (3DP) equipment and bioinks are used to complete bioprinting process. Bioprinting is an interdisciplinary technology that integrates materials science, mechanical design, computer science, and optics [4, 5]. 3DP can be divided into four categories (figure 1): 0D (point-at-once): inkjet-based bioprinting [6–10]; 1D (line-at-once): extrusion-based bioprinting [11–19]; 2D (layer-at-once): digital light processing (DLP) [20–26], continuous liquid interface printing (CLIP) [27] and injection CLIP (iCLIP) [28]; 3D (volume-at-once): computed axial lithography (CAL) [29], which is an emerging 3D (bio)printing paradigm that can print all points of the objects at the same time. The major limitations of traditional bioprinting technologies are slow printing speed and poor surface quality [30]. Vat photopolymerization offers a faster printing speed and a better printing performance by selectively curing light-activated polymer in the vat compares to fused deposition modeling [31]. However, the commonly used ultraviolet (UV) light source in vat photopolymerization process would damage cells, which poses significant obstacles for bioprinting and the following biomedical applications. CAL technology enables printing centimeter-level objects within 30–300 s and resulting a high cell viability, showing great potentials in bioprinting.

The concept of bioprinting is to print with living materials such as cells or bacteria to build biomimetic 3D tissues [34]. The bioprinting process includes three key elements: (1) bioprinting technology; (2)

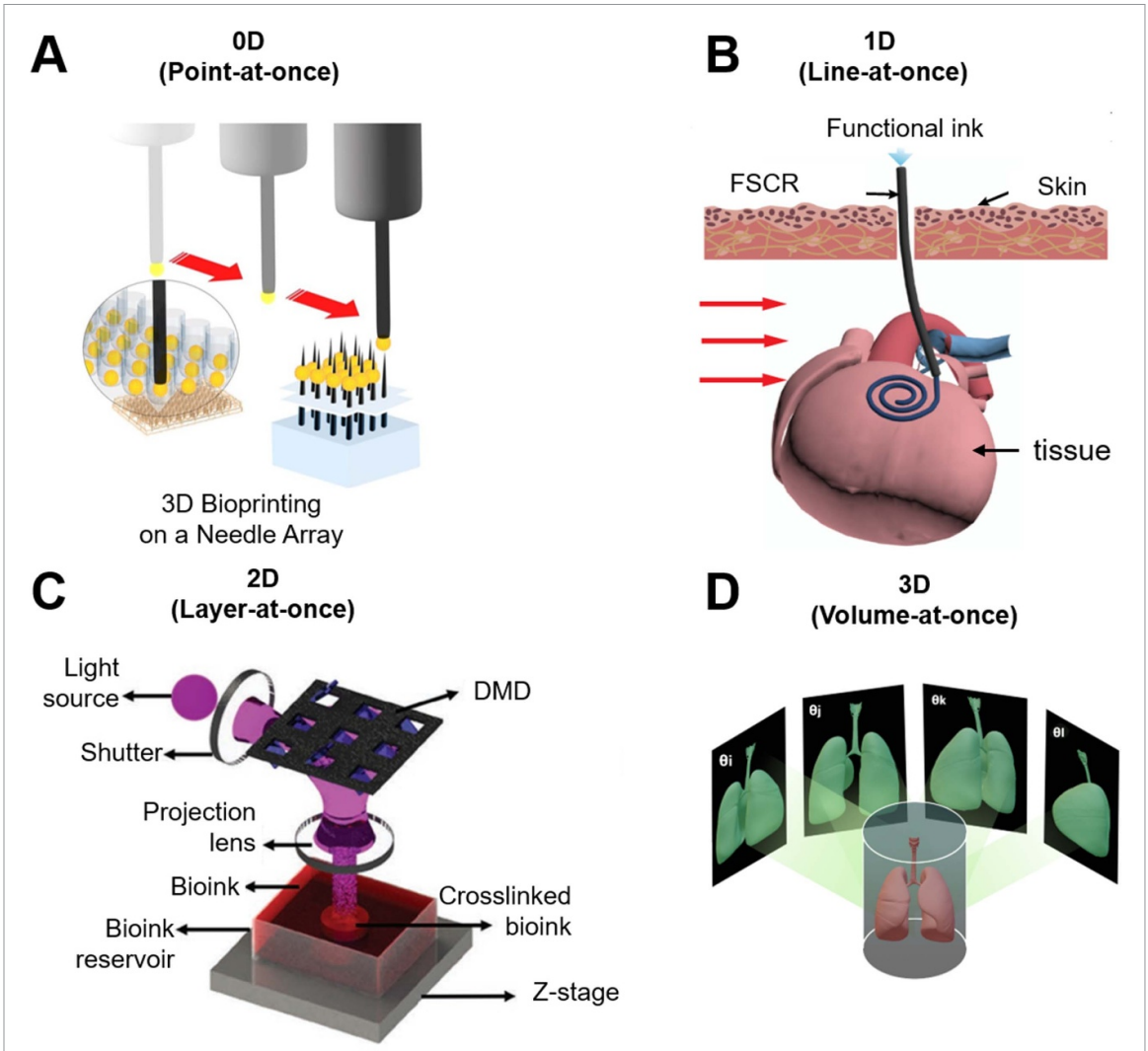

Figure 1. Schematic of 3DP classification in terms of dimensions. (A) Schematic of 0D bioprinting, such as inkjet bioprinting. Reproduced from [10]. CC BY 4.0. (B) Schematic of 1D bioprinting, such as extrusion bioprinting. Reproduced from [32]. CC BY 4.0. (C) The digital light processing (DLP) printing process such as DLP. [33] John Wiley & Sons. © 2019 WILEY-VCH Verlag GmbH & Co. KGaA, Weinheim. (D) Schematic of VBP. Printing all points of entire object simultaneously such as CAL. DLP: digital-light processing. CLIP: continuous liquid interface printing. iCLIP: injection continuous liquid interface production. CAL: computed axial lithography. DMD: digital micromirror device. VBP: volumetric bioprinting.

bioinks; (3) post-treatment and culturing of 3D living constructs. Long bioprinting time of traditional 3DP would cause stress to cells and compromise cell viability when exposing them in external environment [35, 36]. In contrast, the visible light-activated volumetric bioprinting (VBP) technology could (bio)print sophisticate constructs at a centimeter scale within tens of seconds, which avoids using UV light or high temperature during bioprinting process as well, showing a great potential in biofabrication [37].

In addition, bioinks play an important role in bioprinting as well, due to the physicochemical properties of bioinks would significantly influence the printing fidelity, cell viability and functions [38, 39]. Notably, compared with bioinks used in traditional layer-by-layer bioprinting technologies, the bioinks used in VBP could be used at ultra-low concentrations, which broadens choices and expanding the bioink bank. However, the bioinks for VBP still have some special requirements, such as excellent light penetration performance and appropriate viscosity [40].

In this review, the recent development of VBP and related technologies in terms of their working rationale and hardware designs are summarized. Then we focus on the advances in (bio)inks for VBP, followed by further discussion of their biomedical applications. At last, the limitations and future directions of VBP are discussed. Table 1 provides a list of abbreviations used in this review.

2. Printing principle and instrumental design of VBP

The concept of VBP was first proposed by Shusteff *et al* group in 2017, which was inspired by holography (figure 2(A)). It projected beams from three directions to the resin to cure the photopolymer

Table 1. List of abbreviations.

Abbreviation	Full name	Abbreviation	Full name
VBP	Volumetric bioprinting	GelMA	Gelatin methacryloyl
VAM	Volumetric additive manufacturing	BPAGDA	Bisphenol A glycerolate (1 glycerol/phenol) diacrylate
3DP	3D printing	PEGDA	Poly (ethylene glycol) diacrylate
FDM	Fused deposition modeling	CQ	Photoinitiator camphorquinone
SLA	Stereolithography	EDAB	Ethyl 4-dimethylaminobenzoate
SLS	Selective laser sintering	DCPI	Dual-color photoinitiator
SLM	Selective laser melting	SiOC	Silicon oxycarbide
DLP	Digital-light processing	BDDA	1,4-Butandiol-diacrylate
CLIP	Continuous liquid interface printing	TPO	Diphenyl-(2,4,6-trimethylbenzoyl)-phosphinoxide
iCLIP	Injection continuous liquid interface production	PCP	Preceramic polymer
CAL	Computed axial lithography	PDC	Polymer-derived ceramic
UV	Ultraviolet	Gel–NB	Gelatin–norbornene
CT	Computed tomography	PEG4SH	4-Arm-PEG-thiol
DMD	Digital micromirror device	DODT	3,6-Dioxa-1,8-octanedithiol
MEMS	Micro-electromechanical system	CA	Carbic anhydride
SLMs	Spatial light modulators	C2C12	Mouse myoblasts
CGH	Computer-generated hologram	Micro-CAL	Microscale computed axial lithography
STL	Stereolithography	AI	Artificial intelligence
CAD	Computer aided design	ABS	Acrylonitrile butadiene styrene
DCP	Dual-color photopolymerization	hbMSCs	Human bone marrow-derived mesenchymal stromal cells
LAP	Lithium phenyl-2,4,6-trimethylbenzoyl phosphinate	GFP-HUVECs	Green fluorescent human umbilical vein endothelial cells
PI	Photoinitiator	MEW	Melt electrowriting
SS	Silk sericin	Co	Coinitiator
SF	Silk fibroin	ALP	Alkaline phosphatase

simultaneously [41]. Then, Taylor *et al* group drew inspiration from the image reconstruction procedure of computed tomography (CT) and developed CAL system to fabricate 3D parts (figure 2(B)) [42, 43]. In 2020, Loterie *et al* group designed an integrated feedback system to improve the printing resolution of CAL (figure 2(C)), which could produce centimeter-scale structures with 80 μm positive resolution and 500 μm negative resolution within 30 s [44]. Xolography, the linear volumetric 3DP system (figure 2(D)), is different from the previous volumetric systems, uses a dual beam to cure photoresin and achieve a resolution approximately ten times higher than CAL [45].

2.1. *CAL system for* (*bio*)*printing*

In 2019, Kelly *et al* group developed a CAL technology [42], which includes three components: a light source, a platform, and a rotational vial (figure 3(A)). The principle of CAL technology is inspired by the CT

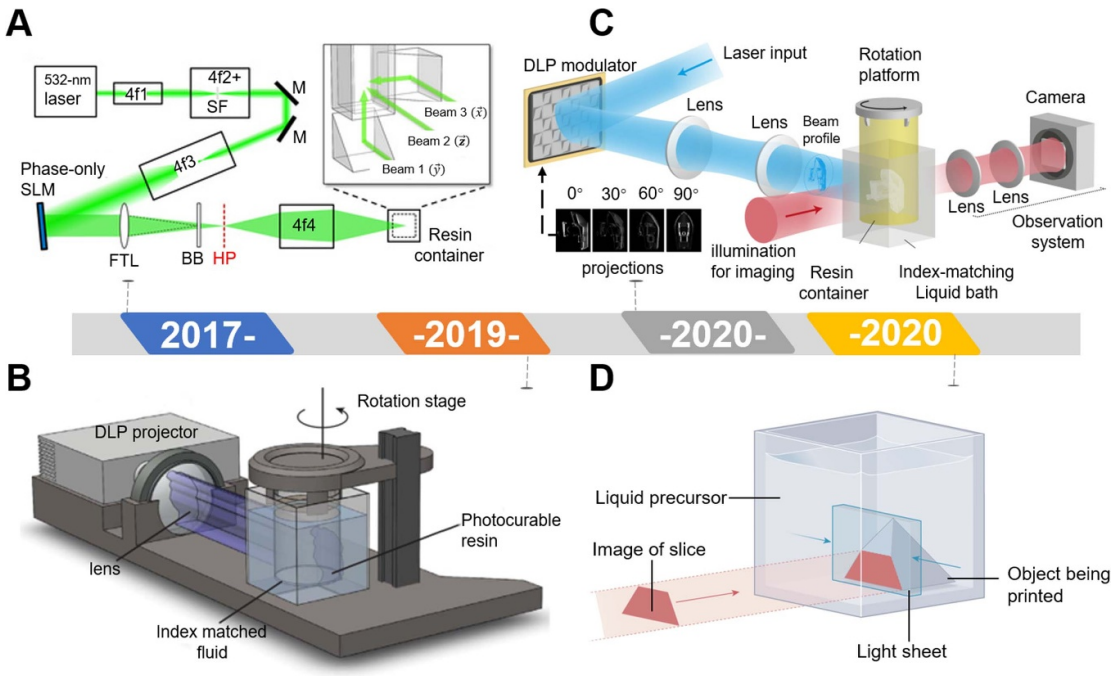

Figure 2. Development of VBP and related bioprinting techniques. (A) Schematic of holographic volumetric 3D fabrication system [41]. From [41]. © 2017 The Authors, some rights reserved; exclusive licensee AAAS. Distributed under a CC BY-NC 4.0 license. Reprinted with permission from AAAS. (B) Schematic of CAL volumetric 3D fabrication system. From [42]. Reprinted with permission from AAAS. (C) Schematic of high-resolution tomographic 3D fabrication system. Reproduced from [44]. CC BY 4.0. (D) Schematic of xolography 3D fabrication system. Reproduced from Darkes-Burkey and Shepherd [46], with permission from Springer Nature. SLM: spatial light modulators. FTL: Fourier-transform lens. BB: beam block. HP: hologram plane. M: mirror. DLP: digital-light processing. CAL: computed axial lithography. VBP: volumetric bioprinting.

image reconstruction procedure. At the time of printing, DLP projects a set of 2D images from different angles into the synchronized rotating resin container. The photosensitive resin would solidify at the designed position after obtaining superimposed illumination from multiple angles. The physical setup system consists of three main parts: DLP projector [47], lens, and printing platform. The printing platform consists of a cylindrical glass vial (1–5 cm in diameter) and a stepper motor. The motor would rotate the cylindrical glass vial at a rotation rate of 3–25° s^{-1} while printing. This system could fabricate centimeter-level constructs within 30–300 s. There are six steps to do to print an ideal model, for example, *The Thinker* (figure 3(B)): (i) imports the standard stereolithography file format (.stl) and slices the target geometry $f_t(r,z)$ (figure 3(C)); (ii) the inverse Radon transform (figure 3(D)) and Fourier transform (figure 3(E)) algorithms are used to compute projection intensities of each z slice; (iii) high pass back-projection filter algorithm is applied to truncate negative information; (iv) the heuristic algorithm is used to iterative optimization projection images to make printed geometry $f(r,z)$ closely simulate the desired target geometry $f_T(r,z)$; (v) the optimized images are projected into photoresin container; (vi) completes the printing and rinses out the construct.

2.2. *High-resolution volumetric manufacturing system for (bio)printing*

To improve the (bio)printing resolution and stability of CAL, Loterie *et al* group designed a high-resolution VBP system (figure 2(C)) [44]. The printing principle is similar to CAL system. The main difference between high-resolution VBP system and CAL system is the addition of a feedback system, which can image the (bio)printing process and accurately control the next (bio)printing process. In detail, a camera was placed at a 90° relative to the projection direction to record the formation of target object in the vial. The first recorded images were used to adjust exposure time and intensity in the second-time (bio)printing process. The obtained construct could achieve a positive feature of 80 μm and a negative feature of 500 μm through this correction [44]. The optimization process needs seven steps (figure 4(A)): (i) a camera was used to record the (bio)printing images (figure 4(B)) of pro-exposure resin vial and defined as $I_{bg}(x',z',\theta)$, which was crucial for next optimal computation; (ii) recording the corresponding angle of each image during exposure and defined as $I_{rec}(x',z',\theta,n)$; (iii) calculating the difference of recordings during exposure and background images:

$$I_{diff}(x',z',\theta,n) = I_{bg}(x',z',\theta) - I_{rec}(x',z',\theta,n) \quad (1)$$

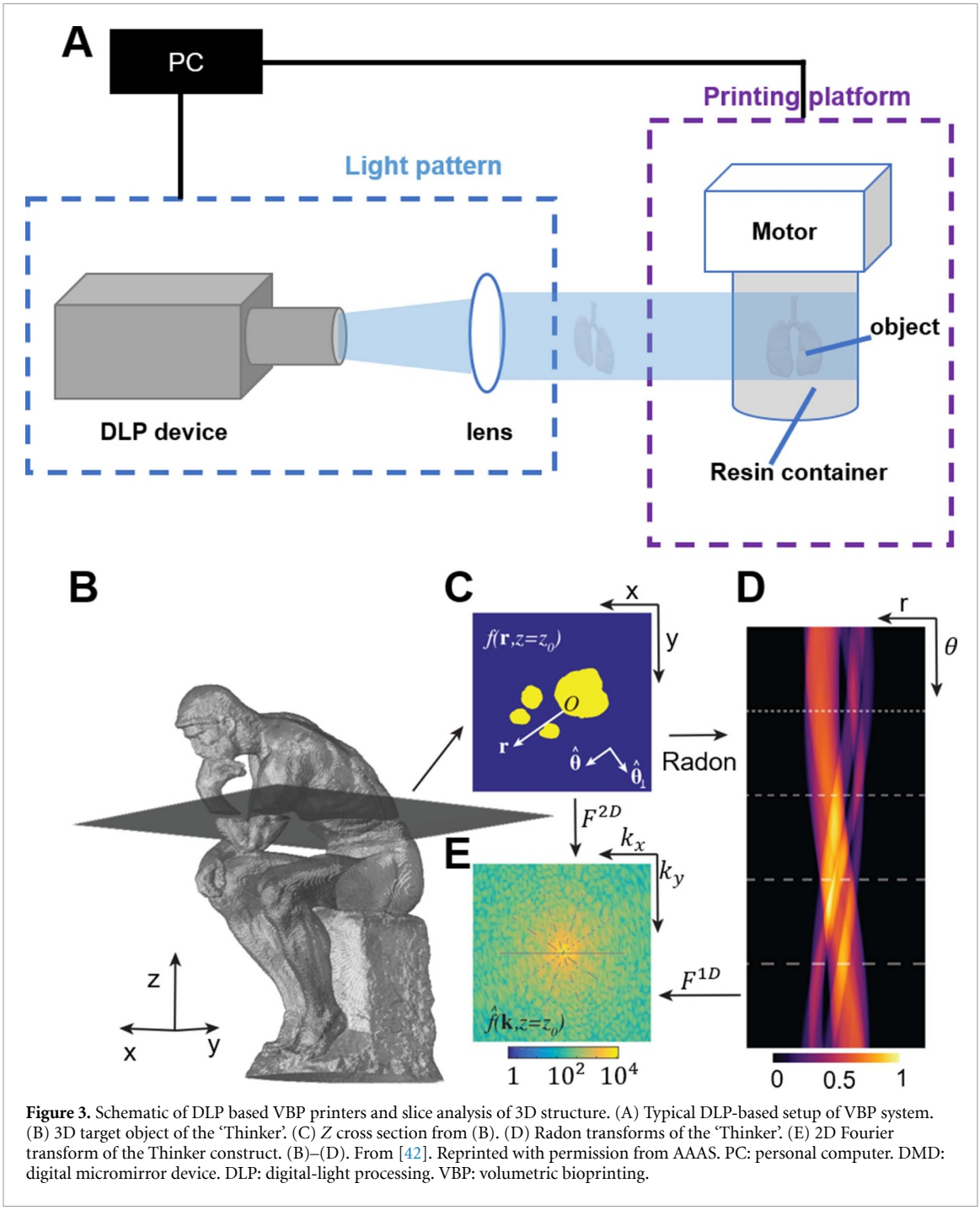

Figure 3. Schematic of DLP based VBP printers and slice analysis of 3D structure. (A) Typical DLP-based setup of VBP system. (B) 3D target object of the 'Thinker'. (C) Z cross section from (B). (D) Radon transforms of the 'Thinker'. (E) 2D Fourier transform of the Thinker construct. (B)–(D). From [42]. Reprinted with permission from AAAS. PC: personal computer. DMD: digital micromirror device. DLP: digital-light processing. VBP: volumetric bioprinting.

(iv) Setting threshold $T = \frac{1}{3}\max I_{\text{diff}}$ to detect changes compared to empty vial images:

$$I_{\text{thresh}}(x', z', \theta, n) = \begin{cases} 1 \text{ if } I_{\text{diff}}(x', z', \theta, n) > T \\ 0 \text{ elsewhere} \end{cases} \quad (2)$$

(v) Arranging exposure images in chronological order and finding out the time and angle of over-cured and uncured successfully:

$$t_{\text{Poly}}(x', z', \theta) = \min_n \{t(n, 0) \,|\, \forall n' \geqslant n : I_{\text{thresh}}(x', z', \theta, n)\} \quad (3)$$

(vi) Using following formula to back-projection polymerization times in 3D:

$$t_{3D}(x, y, z) = \max_\theta \left\{ t_{\text{poly}} \left(x\cos\theta - y\sin\theta, z, \tan^{-1}(y, x) \right) \right\} \quad (4)$$

(vii) Using the map of the polymerization times to modulate voxels that increase or decrease dosage in time and position of uncured or over-cured in next printing process. Finally, a mouse pulmonary artery model (figure 4(C)) and a hearing aid shell model (figure 4(D)) was printed to verify the performance of the feedback system.

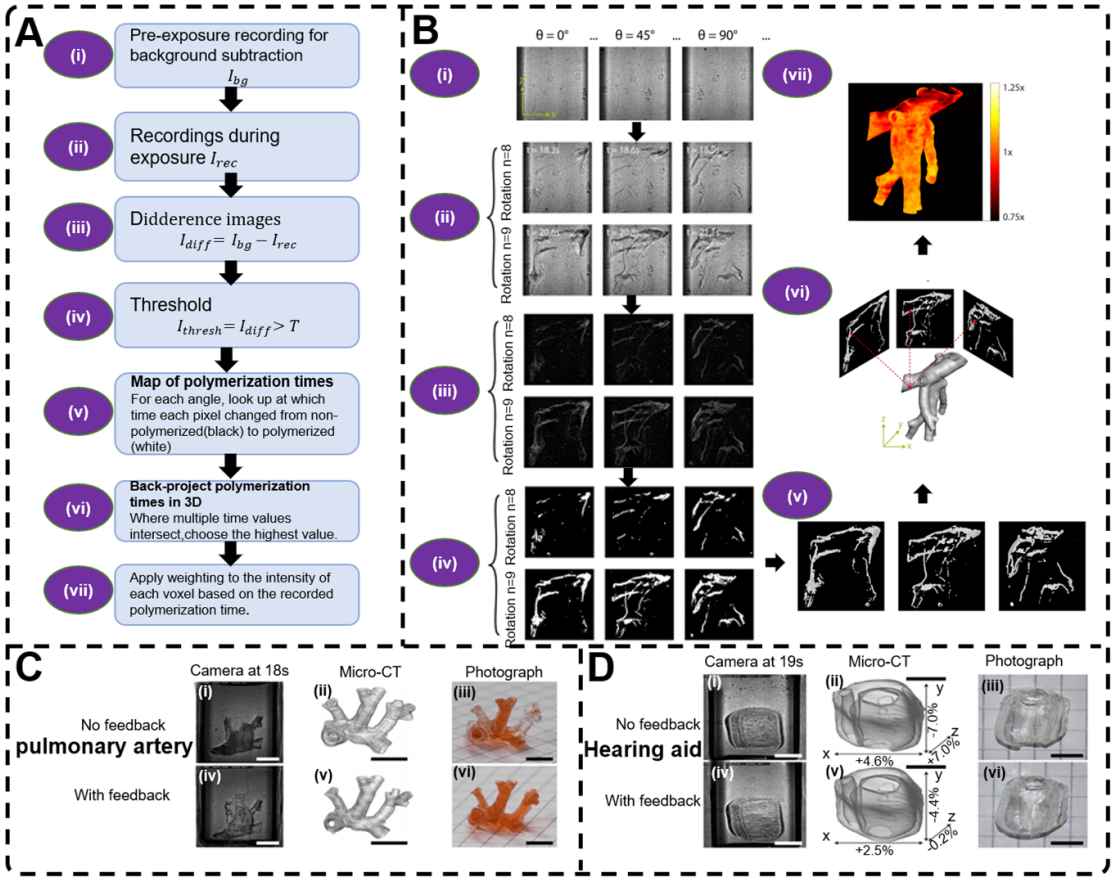

Figure 4. Improvement in VBP accuracy with an integrated feedback system. (A) Schematic of the data processing for a vessel model [44]. Reproduced from [44]. CC BY 4.0. (i) Recording the background images of empty bottle (I_{bg}). (ii) Recording the images during printing (I_{rec}). (iii) Computing the difference of background images and printing images ($I_{diff} = I_{bg} - I_{rec}$). (iv) Setting the threshold of background images ($I_{thresh} = I_{diff} > T$). (v) Sorting the polymerization images by time. (vi) The recording images was back-projected in 3D to detect material in what time and position to solidify. (vii) Dose add or reduction in the next print depending on the solidify information of step (vi). (B) The images were recorded by the camera at different time points corresponding to (A). (i) The images of printing vial at the beginning. (ii) The images of resin printing. (iii) The different value images (I_{diff}). (iv) The images of the changes compared to the empty printing vial after setting the threshold. (v) The images of resin polymerization. (vi) Back-project polymerization times in 3D. (vii) Weighting method was applied to the intensity of each voxel based on the recorded polymerization. (C) The model of mouse pulmonary artery with and without feedback. (D) The model of hearing aid with and without feedback. (B)–(D). Reproduced from [43]. CC BY 4.0.

Further, Antony Orth *et al* group used a new imaging modality called optical scattering tomography in VBP, which could visualize and quantitatively measure the (bio)printing constructs [48]. Their work paves a way for real-time defect detection and correction of high-fidelity tissues and organs (bio)printing.

2.3. *Dual-color photopolymerization system for (bio)printing*

Xolography, different from CAL, uses two different light beams to solid target photoresin (figure 2(D)). Specifically, xolography projects intersecting light beams of different wavelengths to photoswitchable photoresin to solidify localized regions. In detail, the blue light generated by a 375 nm laser, as first wavelength, was used to excite a thin layer of photoinitiator (PI) molecule from its initial dormant state to a potential state with a finite lifetime. Then the orthogonally placed DLP (3840 × 2160 pixels ultra-high definition) projected sliced images onto the plane of potential state of PI molecules to fabricate target model. The method of activating the first wavelength and initiating or inhibiting the polymerization at the second wavelength is called dual-color photopolymerization (DCP) [59]. Xolography has a printing resolution about ten times higher than CAL without a feedback optimization and shows a volume generation rate about 4–5 orders of magnitude higher than two-photon photopolymerization [45].

2.4. Comparison of VBP and other bioprinting techniques

3D bioprinting can be divided into three types: the extrusion-based bioprinting, the inkjet-based bioprinting, and the vat photopolymerization-based bioprinting. VBP is one of vat photopolymerization, which is different from the traditional layer-by-layer printing technology as it could create the whole 3D object at once. VBP is inspired by medical CT imaging algorithm, which offers several advantages such

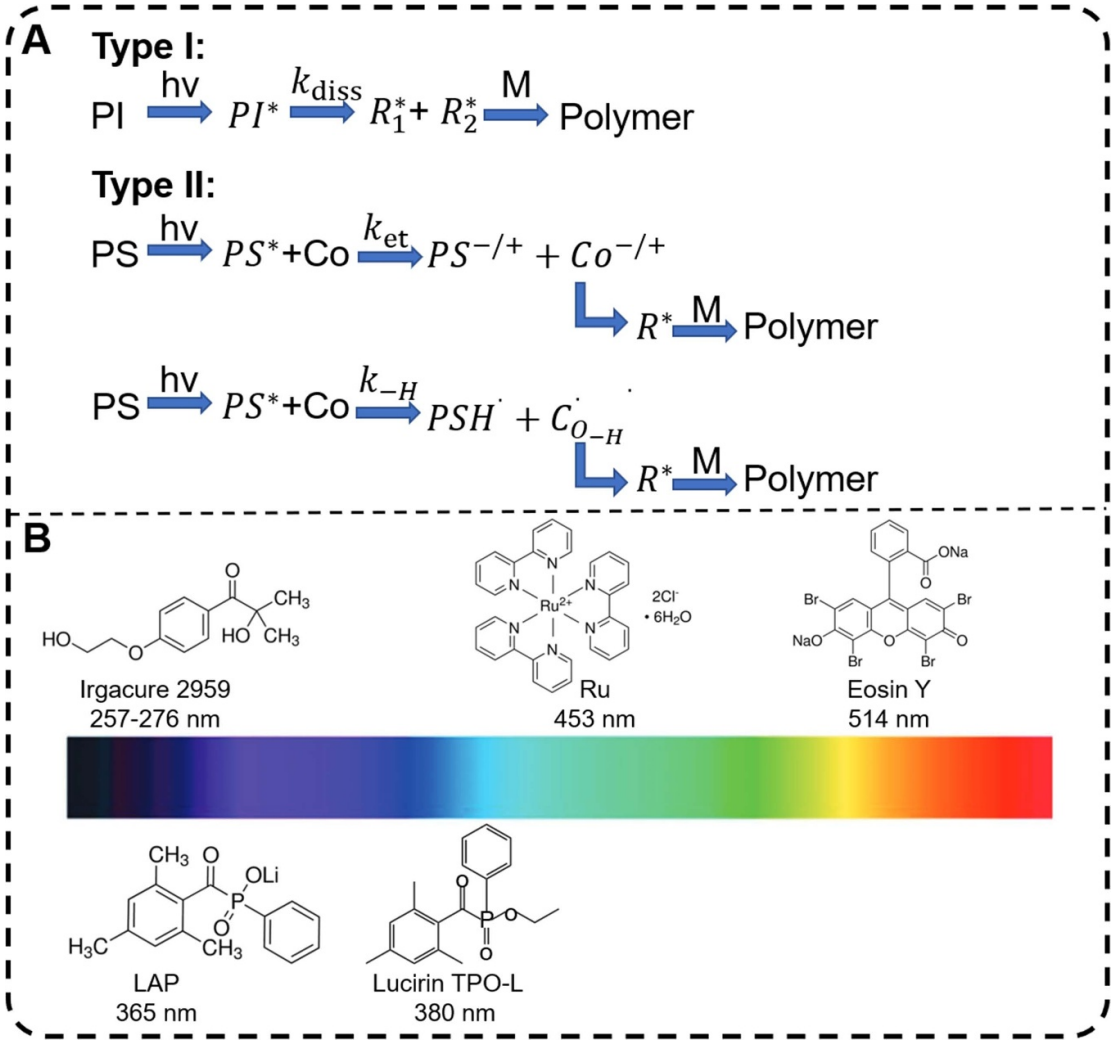

Figure 5. Commonly used type I and type II photoinitiating systems. (A) Two types of photoinitiating systems. PI: photoinitiator, PS: photosensitizer, Co: coinitiator, R*: initiating radical, M: monomer, k_{diss}: rate constant of dissociation, k_{et}: electron transfer rate constant, k_{-H}: hydrogen abstraction rate constant. Reproduced with permission [58]. Copyright 2017, InTech.
(B) Commonly used photoinitiators. Reproduced with permission[31] Copyright 2022, Wiley-VCH GmbH. Irgacure 2959; LAP: lithium phenyl-2,4,6-trimethylbenzoylphosphinate. Ru: Tris(2,2-bipyridyl) dichlororuthenium (II) hexahydrate. Reproduced from [31]. CC BY 4.0. © 2022 The Authors. Advanced Materials published by Wiley-VCH GmbH.

as super-fast printing speed (in tens of seconds), contactless printing mode and high cell survival rate (>95%) [49, 50]. The strengths and limitations of VBP in comparison to other bioprinting techniques are shown in table 3. The contactless, supportless printing modality under visible light and room temperature conditions allowing for more bioprinting scenario than layer-by-layer bioprinting techniques. Meanwhile, the limitations of VBP are included: (i) VBP can only print 3D objects at centimeter-scales (normally less than 10 cm). Increasing the size of printing vial as well as the light intensity and light penetration depths might be one of the solutions. Recently, Christophe Moser group proposed a method called volumetric helical additive manufacturing to print structures up to 3 cm × 3 cm × 5 cm [51, 52]. (ii) Printing resolution is an important indicator in 3DP, creating high-resolution features remains a challenge for VBP. (iii) Multi-material and multi-cellular VBP might be another challenge. (iv) Lack of VBP based (bio)inks. The ideal VBP based (bio)inks should have suitable light penetration depth and excellent biocompatibility.

3. Photoresins for VBP

3.1. PIs and photocrosslinking reactions

PI is a key component for a photopolymerization-based biofabrication modality [53]. Generally, a high concentration of PI would increase the speed of photopolymerization, while might increase the cytotoxicity as well. The commonly used PIs for photopolymerization are classified as type I and type II (figure 5(A)) [54, 55]. Type I PIs are monomolecular, which are the most efficient and commonly used systems in photopolymerization. However, most type I PIs are only reactive under UV light, which

is harmful to cells. The typical I of PIs for biomedical applications includes lithium phenyl-2,4,6-trimethylbenzoylphosphinate (LAP) and Irgacure 2959 (figure 5(B)), both of them can be initiated under 365 nm of wavelength. Type II of PIs are more complex in their initiating reactions than type I PIs, which rely on the combination of two molecules, like tris-bipyridyl-ruthenium (II) hexahydrate (Ru) and sodium persulfate (SPS) [56]. The first molecule absorbs the photon, which is often called the PI or the photosensitizer (PS). The second molecule is often called coinitiator (Co), which gives the initiating radicals (R^*) through photoreaction [57, 58].

Suitable bioinks are needed for bioprinting of high-fidelity and geometrically complex organ structures to match their mechanical stiffness [60]. For example, brain is the utmost excitement of muscle and softest organ of the human body. It is challenging to choose suitable bioinks for bioprinting functional brain model *in vitro* [61].

3.2. (*Bio*)*ink recipes of VBP*

VBP is a new (bio)printing strategy, which lacks suitable (bio)ink. The continuous development of functional (bio)ink would expend the application range of VBP. Bioprinting is to fabricate living constructs for tissue engineering and regenerative medicine, especially in areas such as transplantation and disease modeling [62, 63]. The design of cell compatible bioinks with a high printing performance is a critical step for this perspective. Currently, gelatin methacryloyl (GelMA) is a commonly used bioink in bioprinting [64–67].

Silkworm silk, a natural protein fiber, has an excellent mechanical property and a good biocompatibility. Raw silks mainly contain silk sericin (SS) and silk fibroin (SF) [68–72]. Recently, our group extracted both SS and SF from silkworm (*Bombyx mori*) cocoons and mixed with visible-light PI combination Ru/SPS to prepare SS and SF (bio)inks (figure 6 (A, i)) [49]. For both SS and SF (bio)inks, a variety of complex constructs were volumetrically (bio)printed (figure 6(A, ii and iii)). Interestingly, SS constructs showed a repeated shrinkage and expansion property. And SF constructs with a double-crosslinked network showed tunable mechanical properties (figure 6(A, iv)). The pristine silk-based (bio)inks expend bioinks library of VBP.

Figure 6(B) shows another type of photoclick bioink for fast VBP. First, gelatin–norbornene (Gel–NB) was mixed with a multifunctional crosslinker four-arm-PEG-thiol (PEG4SH). Then 0.05% w/v of LAP was added into the mixture, and UV irradiation was used to crosslink the target structure. PEG4SH was used as a crosslinker to obtain a higher storage modulus than PEG2SH or 3,6-dioxa-1,8-octanedithiol. The carbic anhydride (CA) was used to synthesize Gel–NB, which was cheaper than GelMA. Optorheological studies was performed using 0.05% w/v of LAP, which showed a better cellular compatibility compared with previous reported I2959 [40].

CAL could use engineered polymer resins (such as acrylic polymers and acrylonitrile butadiene styrene polymers) with high viscosities [42]. First, two acrylate polymers bisphenol A glycerolate (1 glycerol/phenol) diacrylate (BPAGDA)/poly (ethylene glycol) diacrylate (PEGDA) (average $Mn = 250\ g\ mol^{-1}$) were mixed at a ratio of 3:1 or 7:1 to form acrylate photopolymers (figure 6(C)). Then two photoinitiating system consisted of 5.2 mM photoinitiator camphorquinone (CQ) and 5.2 mM coinitiator ethyl 4-dimethylaminobenzoate was added to form engineered polymer. This mixture was measured to have a considerably high viscosity of 93 000 $\pm$ 5000 mPa s (7:1 of BPAGDA/PEGDA formulations). The high viscosity indicated that the relative displacement of the print can be reduced during the printing process, which improved the printing fidelity and the printing resolution. The resin was cured by irradiation with 405 nm light source, and the printed structures were stained for easy optical observation (figure 6(C, i–v)).

DCPI is a photoswitch-incorporated photoinitiating system that requires two different light beams to activate [74]. The first step was irradiated with 375 nm of UV light; thus, the irradiated part was widely absorbed at 450–700 nm, and then the (bio)ink was polymerized under 585 nm of red light. The synthesis of DCPI was divided into three steps (figure 6(D)): first, the syntheses of 5-cyano-1,2,3,3-tetramethylindolenium iodide and 4-fluoro-3′-formyl-4′-hydroxybenzophenone; then 5-cyano-1,2,3,3-tetramethylindolenium iodide and piperidine were dissolved in ethanol; finally, 4-fluoro-3′-formyl-4′-hydroxybenzophenone was added to the mixture from step 2 and heated to 70 °C to form DCPI. High resolution (25 μm) was achieved.

Recently, Kollep *et al* group successfully printed ceramic parts using a volumetric printer [73]. The preparation of ink is shown in figure 6(E). The ink consists of three parts: (i) polysiloxane (SPR 684) was as a preceramic polysiloxane resin; (ii) 1,4-butandiol-diacrylate was as a crosslinker; (iii) diphenyl-(2,4,6-trimethylbenzoyl)-phosphinoxide was as a photoinitiator. The crosslinked preceramic was formed by irradiation with 405 nm of blue light source about 1 min. Then, the green body (CAL-printed structure without debinding and sintering) was converted to polymer-derived ceramic (PDC) during pyrolysis at 1000 °C for 48 h. Polysiloxane (SPR 684) is a commercially available material that can be pyrolyzed into ceramics at 1000 °C–2000 °C [75]. The viscosity of the ink was 873 mPa s. In short, the process started with a liquid preceramic polymer, which was solidified into a green body. Then the green body was

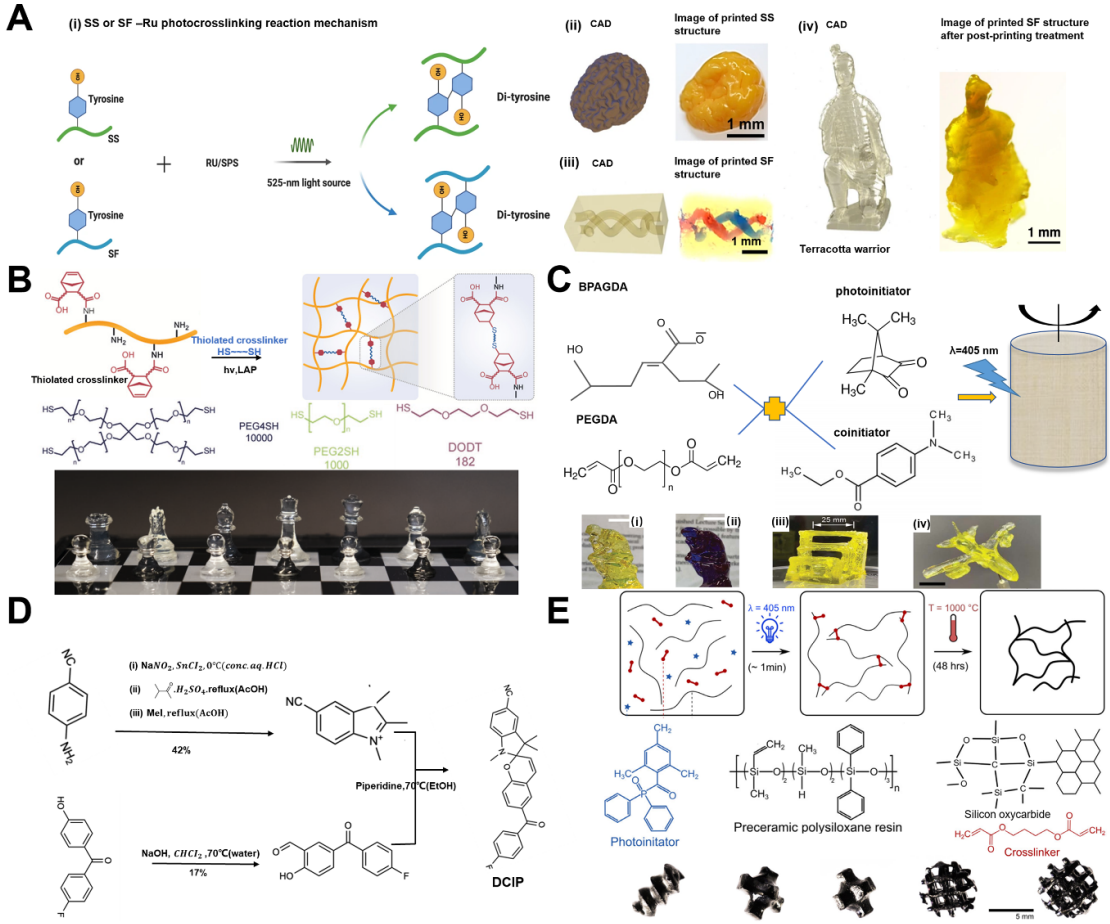

Figure 6. Synthesis process of commonly used photoresins for VBP. (A) (i) Schematic of silk-based materials (SS or SF)/Ru-SPS photocrosslinking reaction mechanism and printed structures. (ii) Brain-like construct (2.5% SS with 0.5 mM Ru/5 mM SPS). (iii) Dual spiral channel construct (5% SF with 0.25 mM Ru/2.5 mM SPS). (iv) Terracotta warrior construct (2.5% SF, 0.5 mM Ru/5 mM SPS). Reproduced from [49]. CC BY 4.0. (B) Schematic of thiol–ene based photoresin, which composed of gelatin–norbornene (Gel–NB) and a thiolated crosslinker. Upon 405 nm excitation with LAP as an initiator, the generation of radical initiation species leads to a step-growth crosslinking mechanism. [40] John Wiley & Sons. © 2021 The Authors. Advanced Materials published by Wiley-VCH GmbH. (C) Schematic of engineering polymers resin synthesis, which was formulated from two commercially available acrylate photopolymers bisphenol A glycerolate (1 glycerol/phenol) diacrylate (BPAGDA) and poly (ethylene glycol) diacrylate (PEGDA) mixed with two photoinitiators camphorquinone (CQ) and coinitiator ethyl 4-dimethylaminobenzoate (EDAB). (i)–(v) Structures were printed using BPAGDA/PEGDA photoresins under 405 nm wavelength light source. From [42]. Reprinted with permission from AAAS. (D) Synthesis of dual-color photoinitiator (DCPI). Reproduced from [45], with permission from Springer Nature. (E) Schematic of silicon carbide ceramics synthesis and printed structures. [73] John Wiley & Sons. © 2022 The Authors. Advanced Engineering Materials published by Wiley-VCH GmbH. SS: silk sericin. SF: silk fibroin. Ru: tris-bipyridyl-ruthenium (II) hexahydrate. SPS: sodium persulfate.

transformed to a ceramic material, generally referred to as PDC.

Table 2 shows the currently reported (bio)inks used in VBP, which are divided into two categories: bioink and functional ink. Then, the following part mainly introduces the applications of VBP based on these (bio)inks.

4. Biomedical applications of VBP-based technology

4.1. Bioprinting

Bernal *et al* group used cell-friendly hydrogel bioink to bioprint large living tissue constructs (figure 7(A)) [77]. Except for using a volumetric printer to print human auricle model (figure 7(A, iii)), they also volumetrically bioprinted meniscal, trabecular, trabecular bone-like constructs, which showed high cell viabilities (>85%) after culturing for 7 d [77]. Bernal *et al* group investigated a new method to explore the optical properties of cell-laden hydrogels for VBP and unraveled the culture of organoid structures and the influence of cell on printing resolution [50]. In terms of cell culture, researchers used tens of millions of cells to bioprint. They set up a dynamic culture system to culture cells isolated from human liver biopsies (figure 7(B)). Essentially, these organoids were epithelial, which was a cyst-like structure with an inner hollow lumen surrounded by a thin cell (mono)layer [50]. These cell-laden structures were volumetrically bioprinted within 20 s and the printed organoids were used as biofactories in established sterile perfusion

Table 2. (Bio)inks investigated in volumetric printing.

Irradiation wavenumber (nm)	Monomers	Photoinitiator and co-initiator	References
525	Silk sericin	Tris-bipyridyl-ruthenium (II) hexahydrate, sodium persulfate	[49]
525	Silk fibroin	Tris-bipyridyl-ruthenium (II) hexahydrate, sodium persulfate	[49]
385	Poly(ethylene glycol) diacrylate	Lithium phenyl-2,4,6-trimethylbenzoylphosphinate	[76]
405	Gelatin; carbic anhydride	Lithium phenyl(2,4,6-trimethylbenzoyl) phosphinate	[77]
365	GelMA	Lithium phenyl(2,4,6-trimethylbenzoyl)phosphinate	[50, 78]
Blue light at ∼455	Glycerolate diacrylate	Camphorquinone; photoinitiator (PI)	[78]
UV at ∼365	Poly(ethylene glycol) diacrylate;	Ethyl 4-dimethylaminobenzoate;	
532	Poly(ethylene glycol) diacrylate	Irgacure 784	[41]
405 blue color channel	Bisphenol A glycerolate (1 Glycerol/phenol) diacrylate Poly(ethylene glycol) diacrylate	Camphorquinone Ethyl 4-dimethylaminobenzoate	[42]
405 green color channel	Gelatin methacrylate	Tris(2,2bipyridyl) dichlororuthenium(II) hexahydrate Sodium persulfate	[42]
405	Di-pentaerythritol pentaacrylate	Phenylbis(2,4,6-trimethylbenzoyl)phosphine oxide	[44]
375	Pentaerythritol tetraacrylate	5-Cyano-1,2,3,3-tetramethylindolenium iodide	[45]
From 450 to 700		4-Fluoro-3′-formyl-4′-hydroxybenzophenone	
375	Diurethane dimethacrylate	5-Cyano-1,2,3,3-tetramethylindolenium iodide	[45]
From 450 to 700		4-Fluoro-3′-formyl-4′-hydroxybenzophenone	
375	Diurethane dimethacrylate	5-Cyano-1,2,3,3-tetramethylindolenium iodide	[45]
From 450 to 700	2-hydroxyethy lmethacrylate	4-Fluoro-3′-formyl-4′-hydroxybenzophenone;	
442	Trimethylolpropane ethoxylate triacrylate Hydroxyethylmethacrylate	Camphorquinone Ethyl 4-(dimethylamino)benzoate	[79]

(Continued.)

chambers, opening a new possibility for the future development of self-sustaining biofactories.

Rizzo *et al* group volumetrically bioprinted a cell-laden branch model of mesoscale vessel lumen size (figure 7(C, i)) [40]. In this study, the capsulated mouse myoblasts muscle cells (C2C12) were used to proliferate, spread, and differentiate into multinucleated contractile myotubes in a soft crosslinked matrix (figure 7(C, ii)), which showed a distinguished cell viability (>95%) upon printing and >90% after 7 d of culture; meanwhile, the differentiation of myotubes was observed after 3 weeks of culture (myosin heavy chain: red, nuclei: blue, scale bars: 200 μm) (figure 7(C, iii)) [40]. The study showed that VBP had the ability to generate complex tissue models such as skeletal muscle with a high-throughput potential.

In our recent study, our group showed that both SS and SF (bio)inks could be volumetrically bioprinted as low as 2.5% (figure 7(D)) [49]. The cell-laden silk (bio)inks (2.5% and 5% SS, 0.5 mM Ru/5 mM SPS; 2.5%–10% SF with a single photocrosslinked

Table 2. (Continued.)

Irradiation wavenumber (nm)	Monomers	Photoinitiator and co-initiator	References
		2,2,6,6-tetramethyl-1-piperidinyloxy	
405	Polysiloxane 1,4-Butandiol-diacrylate	Diphenyl-(2,4,6-trimethyl benzoyl)-phosphinoxide	[73]
405	Gelatin methacryloyl	Lithium phenyl-2,4,6-trimethylbenzoyl phosphinate	[80]
405	Di-pentaerythritol pentaacrylate	Phenylbis(2,4,6-trimethylbenzoyl)phosphine oxide	[40]
405	Aliphatic urethane diacrylate	Phenylbis(2,4,6-trimethylbenzoyl)phosphine oxide	[40]
405	Vinyl-terminated PDMS 62 kg mol^{-1} Fumed silica reinforced vinyl-terminated (Mercaptopropyl)Methylsiloxane-dimethylsiloxane	Ethyl (2,4,6-trimethylbenzoyl) phenylphosphinate	[81]
460	Bisphenol A glycerolate diacrylate Poly(ethylene glycol) diacrylate	Camphorquinone Ethyl 4-dimethylaminobenzoate	[80]
405	Urethane dimethacrylate IPDI	2-Methyl-4-(methylthio)2-morpholinopropiophenone	[82]
405	Bisphenol A glycerolate diacrylate; poly(ethylene glycol) diacrylate	Irgacure 907 -Methyl-4′-(methylthio)-2-morpholinopropiophenone	[83], [84]
405	Tri-allyl isocyanurate Tris[2-(3-mercaptopropionyloxy)ethyl] isocyanurate	Irgacure 907 2,2,6,6-tetramethyl-1-piperidinyloxy	[83]

network, 0.25 mM Ru/2.5 mM SPS) showed favorable cytocompatibility. Specifically, both 2.5% SS and 2.5% SF constructs supported better proliferation rates and viability than constructs with higher silk concentrations. The cytocompatibility of SS and SF bioinks at low-concentrations (2.5%–5%) made them suitable for VBP applications where living cells are encapsulated. Of note, unlike SF.

Gehlen *et al* group volumetrically bioprinted a centimeter-scale heterocellular bone model contained human mesenchymal stem cells (hMSCs) and co-cultured with human umbilical vein endothelial cell (HUVECs); and the 3D osteocyte was successful differentiated after 42 d of culture [78]. In detail, first, a bioink (5% GelMA, 0.05% LAP, hMSCs) was prepared to bioprint a pre-vascularized bone construct (figure 8(A, i and ii)). After culturing 7 d, the HUVECs cell suspension was injected into a hollow channel (figure 8(A, iii)). Figure 8(B) showed that the confocal 3D image after co-culture of 7 d, the red color shows the self-organized endothelial monolayer in lining of channels. Meaningfully, after 3D co-culture of 42 d, the osteoblastic markers (collagen-I, alkaline phosphatase (ALP), osteocalcin) and osteocytic markers (podoplanin; dentin matrix acidic phosphoprotein 1) were expression.

Cell concentration would affect resolution of VBP. Thus, it is necessary to explore how to bioprint high-fidelity tissue structures in a high concentration or turbid bioinks. Madrid-Wolff *et al* group used scattering corrected VBP method to manufacture cell-laden complex geometry constructs [80]. As a proof-of-concept, the vasculatures with four hollow channels (the bioink contained 4×10^6 ml^{-1} of human embryonic kidney 293 cells), which was challenging, were successfully volumetrically bioprinted (figure 8(C)), expending the potential of biomedical applications of VBP.

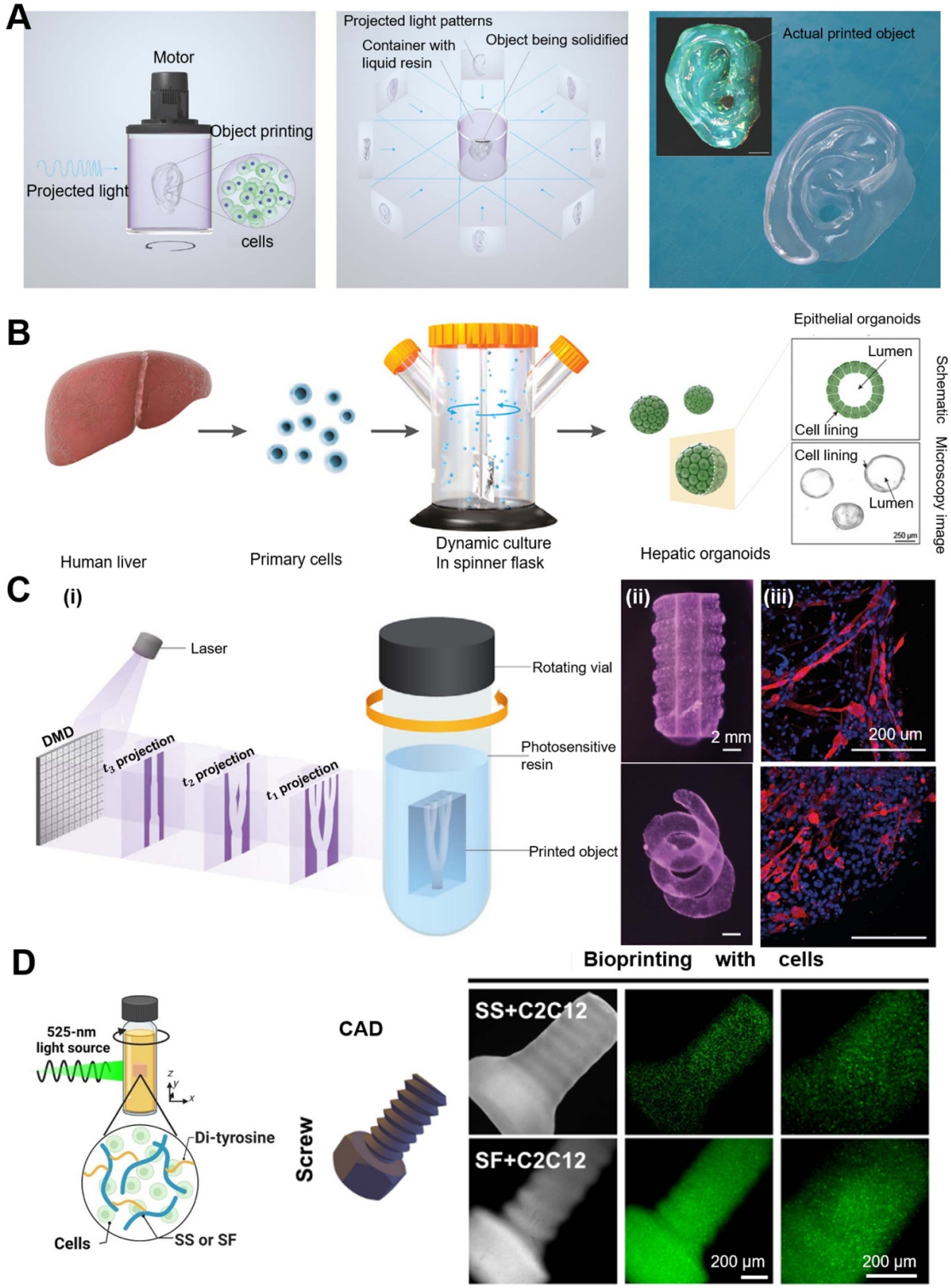

Figure 7. Biomedical applications of VBP. (A) The cochlear model was volumetrically bioprinted with a resin mixed with equine tissue samples and cells (stained with Alcian blue to facilitate visualization). [77] John Wiley & Sons. © 2019 The Authors. Published by WILEY-VCH Verlag GmbH & Co. KGaA, Weinheim. (B) Schematic of a hepatic organoid culture system, cells were isolated from human liver biopsies, which were then dynamically cultured in a spinner flask system to establish high yields of hollow epithelial organoid structures (microscopy image scale bar = 250 μm). Reproduced from [50]. CC BY 4.0. © 2022 The Authors. Advanced Materials published by Wiley-VCH GmbH. (C) (i) Schematic of volumetrically printed a vessel branch model. (ii) Volumetrically bioprinted a C2C12-laden complex free-form object. (iii) Immunofluorescence images of volumetrically bioprinted myotubes differentiation after 3 weeks of culture (myosin heavy chain: red, nuclei: blue, scale bars: 200 μm) [40]. John Wiley & Sons. © 2021 The Authors. Advanced Materials published by Wiley-VCH GmbH. (D) Volumetrically bioprinted SS and SF constructs embedded with mouse myoblasts C2C12 cells. Reproduced from [49]. CC BY 4.0. SS: silk sericin. SF: silk fibroin. C2C12: mouse myoblasts. VBP: volumetric bioprinting.

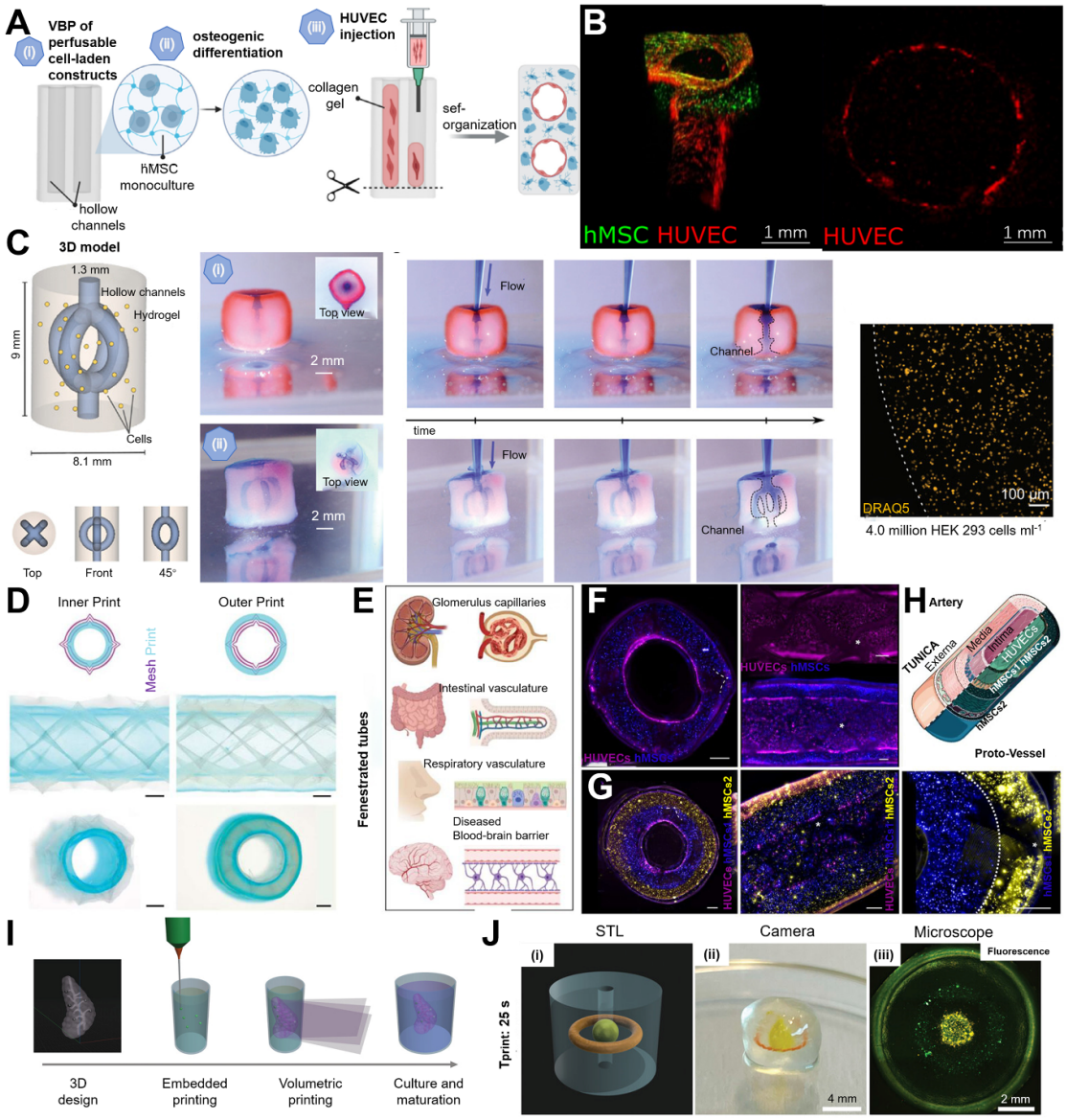

Figure 8. Biomedical applications of VBP. (A) (i) Volumetrically bioprinted hMSC-laden hollow pre-vascularization model and cultured for 6 d. (ii) The HUVECs suspension was injected into the hollow channels. (iii) Schematic of heterocellular perfusable pre-vascularization model after 14 d of culture. (B) The 3D confocal image of a hollow pre-vascularization model on 14 d of culture, hMSCs were stained with calcein-AM (green) and HUVECs were stained with DiD (red). (a), (b) Reproduced from [78]. CC BY 4.0. (C) The scattering-corrected VBP method permits printing complex hollow channels with high concentration bioink contained 4×10^6 human embryonic kidney 293 cells ml^{-1}. (i) The blue dye could not pass through channels without scattering correction. (ii) The blue dye could pass through channels using scattering corrected VBP. Reproduced from [80]. CC BY 4.0. © 2022 The Authors. Advanced Science published by Wiley-VCH GmbH. (D) VBP across melt electrowritten technology was successfully used to manufacture intricate, multi-material and mechanical stability tubular structures, and could be used to volumetrically print structures inner or outer of MEW mesh. (E) VBP across melt electrowritten technology could be used to print various fenestrated structures of native tissues/structures. (F) Two-layer VBP across melt electrowritten technology could be used to bioprint tubular constructs with hMSCs (blue) and HUVEC (magenta). Scale bar: 500 μm. (G) Three-layer VBP across melt electrowritten technology could be used to bioprint tubular construct hMSCs (blue and yellow) and HUVEC (magenta). Scale bar: 500 μm. (H) Schematic of proto-vessel. (D)–(H) Reproduced from [81]. CC BY 4.0. © 2023 The Authors. Advanced Materials published by Wiley-VCH GmbH. (I) Sequential of extrusion-VBP combined printing. (J) VBP of complex co-culture model. (i) STL file. (ii) Optical image of the printed structure. (iii) Microscope image of the printed structure. Reproduced from [85]. CC BY 4.0. © 2023 The Authors. Advanced Materials published by Wiley-VCH GmbH. VBP: Volumetric bioprinting. hbMSCs: human bone marrow-derived mesenchymal stromal cells. HUVECs: human umbilical vein endothelial cells. MEW: melt electrowriting.

4.2. VBP of multi-material and multi-cell

VBP of multiple-material and multiple-cell is important, challenging as well, for heterogeneous tissue-like structures, and some laboratories have made some progresses [86–88].

By cooperating with other 3DP technologies, VBP has brought some exciting results in heterogeneous tissue-like structures, such as multicellular blood vessel model and localized high-density cell bioprinting [81, 85]. Recently, Größbacher *et al* group converged

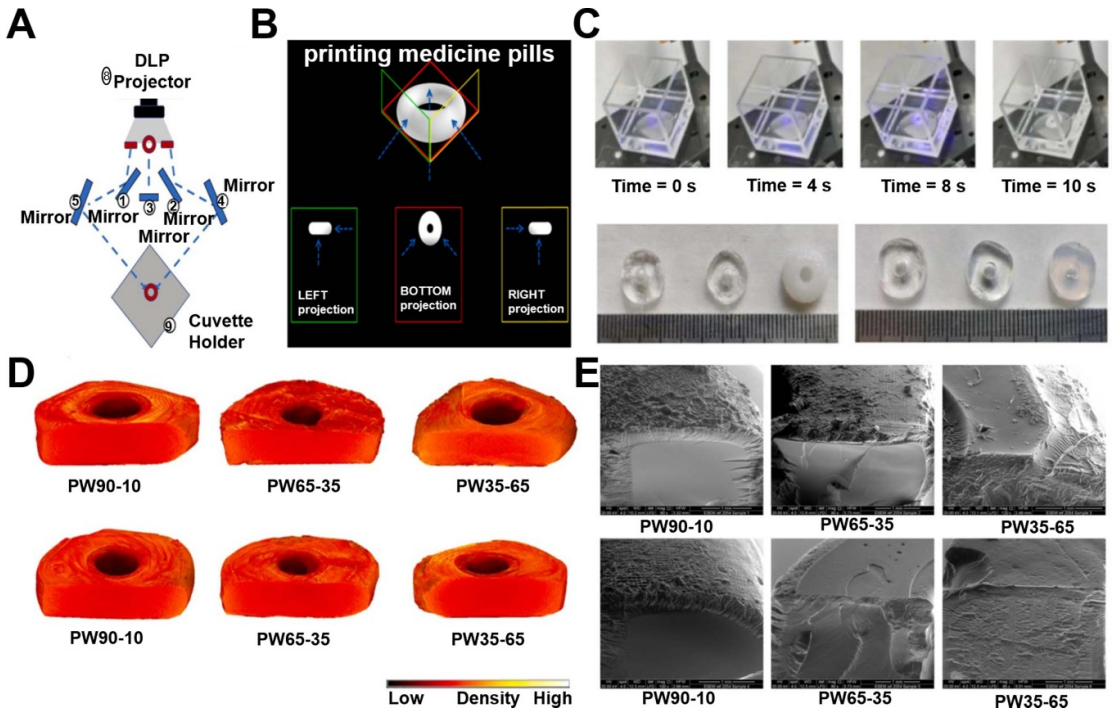

Figure 9. VBP of medicinal pills. (A) Schematic of VBP device. (B) Schematic of the irradiance of photosensitive resin with three orthogonal light beams. (C) Sequential view of the cuvette during the pill fabrication process. (D) X-ray micro-CT images of different pills. (E) Environmental scanning electron microscope (ESEM) images of cross sections of different printed pills. (A)–(E) Reproduced from [93]. CC BY 4.0. VBP: volumetric bioprinting.

VBP with melt electrowriting (MEW) technology to bioprint intricate, multi-material and mechanical stability tubular structures [81]. Interestingly, inter or outer of MEW mesh (figure 8(D)) and micron-scale fenestrations such as permeable vessels in human body (figure 8(E)) could be volumetrically (bio)printed [89, 90]. In detail, the bioprinting process was divided into four steps: (i) MEW mesh architectures with different pore shapes (*i.e.* 34° or 70° winding angles) and thicknesses (*i.e.* 20, 30, 40, 60 printed layers) were fabricated; (ii) the MEW mesh was put into the first bioink container (5% w/v GelMA + 0.1% w/v LAP and 1×10^7 cells ml^{-1} human bone marrow-derived mesenchymal stromal cells (hbMSCs)) to volumetrically bioprinted first layer (1050°μm) hollow tube (outer of MEW mesh) (figure 8(F)); (iii) the sample and re-infused the bioink (5% w/v GelMA + 0.1% w/v LAP and 5×10^5 cells ml^{-1} hbMSCs) was washed and volumetrically bioprinted second layer (800°μm) around first layer (figure 8(G)); (iv) the sample was washed and cultured overnight, then 1×10^7 cells ml^{-1} green fluorescent HUVECs suspension were seeded inner of MEW mesh on the next day, which were rotated 90° every 20 min to create the third layer (80°μm). At last, the researchers merged these two technologies to build a tri-layered cell-laden vessels (figure 8(H)), which expended the potential applications of VBP in vascular tissue engineering.

Riccardo Levato *et al* group converged VBP with extrusion bioprinting technology to print physiologically-relevant models [85]. The characteristic of this hybrid printing technology was permissive high cell densities ($>10^7$ ml^{-1}) printing in a pre-defined spatial location. Specifically, a geometry was printed in a vial filled with bioink using extrusion printer, then this vial was put into a VBP printer to print another intricate geometry with different bioinks (figure 8(I)). Some complex co-culture models like branch vasculature, Einstein's head and pancreatic models were printed (figure 8(J)). The printing time was less 5 min [77, 91].

4.3. VBP of personalized tablets

3DP technology is applicable for pharmaceutical industry, because of its personalized and highly customized manufacturing ability [92]. 3DP technology could be applied to patient-friendly drug development by adjusting drug dose, shape, flavor, and mining release patterns to meet the individual need, showing a great potential in the pharmaceutical industry [76].

Rodríguez-Pombo *et al* group successfully prepared printlets (pills) containing paracetamol within 7–17 s using a volumetric printer, for the first time [93]. It is the fastest way to produce personalized oral pills so far. The printing system could divide a light source into three propagation paths and spread it into the resin container bottle to cure the pill in 10 s (figures 9(A) and (B)). The images of six pills: PW90-10, PW65-35, PW35-65, PP90-10, PP65-35, PP35-65 were shown in figure 9(C). Then the x-ray micro-CT

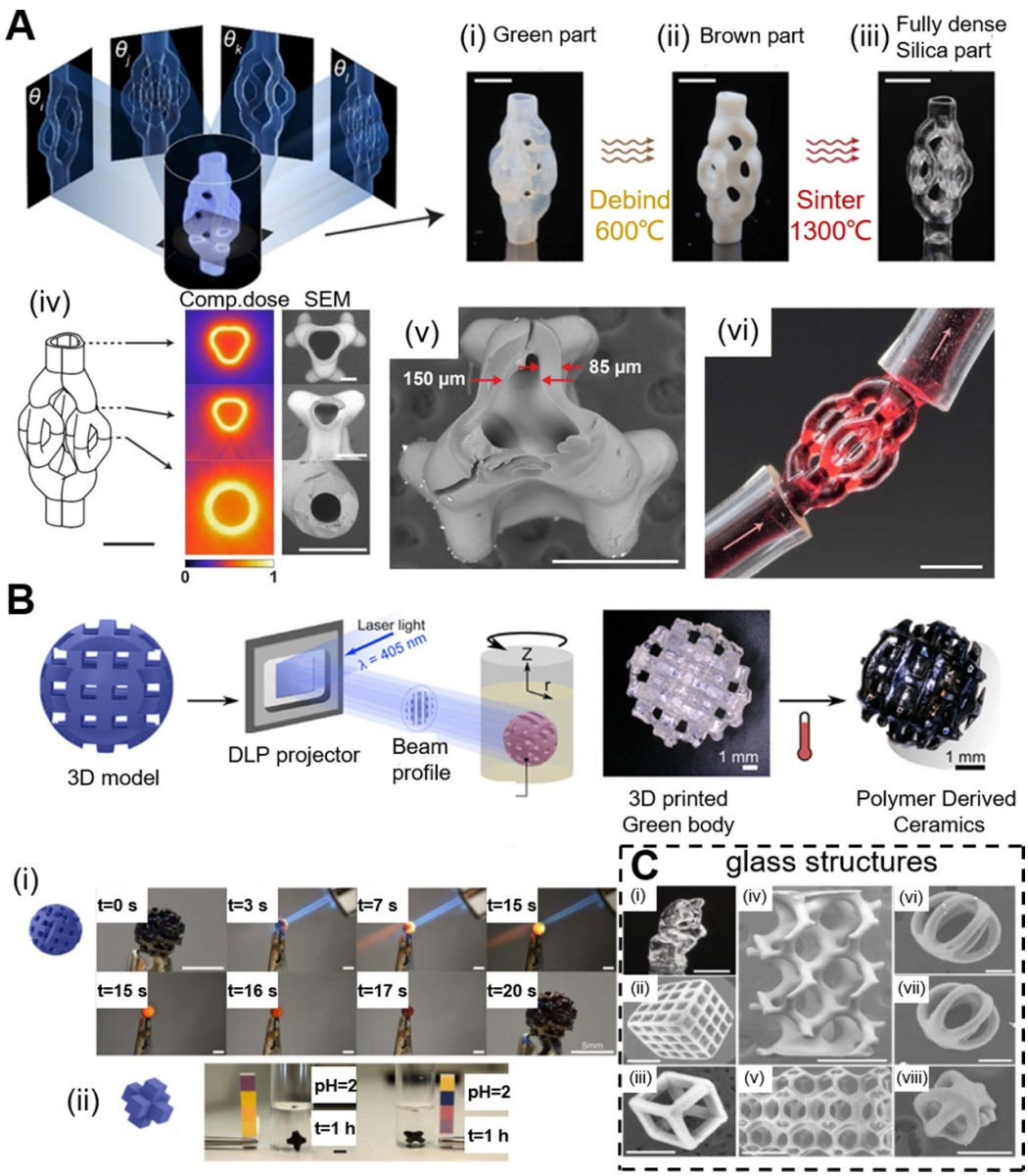

Figure 10. VBP of silicon glass and silicon oxycarbide ceramics. (A) VBP of glass. (i)–(iii) The resulting green parts were subjected to thermal treatment in two steps. Scale bar: 2 mm. (iv)–v) The representative slices of trifurcated channel. (vi) Dye passes through the model channel. Scale bar: 2 mm [79]. From [79]. Reprinted with permission from AAAS. (B) Volumetrically printed silicon oxycarbide ceramics, the 3D model of the desired part was used to calculate a set of light patterns, which were projected onto a rotating vial filled with a photocurable preceramic resin. The resulting solid green body was retrieved from the liquid resin, and pyrolyzed at $T = 1000\ ^{\circ}$C. (i) Resistance of ceramic test with a butane torch (≈1400 °C). (ii) Acid base test for 1°h. [73] John Wiley & Sons. © 2022 The Authors. Advanced Engineering Materials published by Wiley-VCH GmbH. (C) (i) Photograph of a 'Thinker'. (ii) The scanning electron microscope (SEM) micrograph of 4 × 4 cubic lattice. (iii) SEM micrograph of cubic structure. (iv) SEM micrograph of skeletal gyroid lattice. (v) SEM micrograph of tetrakaidecahedron lattice. (vi) SEM micrograph of spherical cage structure. Scale bars: (i)–(v) 1 mm, (vi) 200 μm. From [79]. Reprinted with permission from AAAS. VBP: volumetric bioprinting.

images of different pills (figure 9(D)) and environmental scanning electron microscope images of cross sections of different pills after all processing steps were observed (figure 9(E)). VBP offers a fast way of pharmaceutical development and drug testing, showing unique advantage in personalized medication [94–96].

4.4. VBP of glass

The traditional glass manufacturing process requires complex procedures with a high temperature melting and a casting process, facing great challenges in manufacturing equipment that can arbitrarily produce complex glass [81, 97]. Next, we introduce the application of VBP in manufacturing both silica glass and silicon oxycarbide ceramics.

Toombs *et al* group designed a microscale CAL system [79], which was capable of printing minimum feature sizes of 20°μm for polymer, and minimum feature sizes of 50°μm for fused silica glass. The green body (figure 10(A, i)) was obtained by curing the silica glass nanocomposite resin. Then

Table 3. Comparison of different bioprinting technologies.

Bioprinting technology		Advantages	Disadvantages	Applications	References
Extrusion		• Suitable for heterogeneous tissue structures bioprinting • Suitable for *in situ* and *in vivo* bioprinting	• Relative low printing speed (minutes-hours) • Relative low feature size resolution (>100 μm) • Bioink needs suitable rheological properties	• Tissue engineering • Multi-component and spatially heterogeneous tissues bioprinting • *In situ* bioprinting	[11–17]
Inkjet		• Low cost • Easy to operation and develop	• Easy to clog • Shear stress affects cell viability (70%–90%)	• Drug screening • Drug-loaded vesicles • Scaffold fabrication	[6–9]
Vat photopolymerization	DLP	• High resolution features (10–50 μm) • Possible to create geometrically complex constructs • The ability to integrate multiple bioresins to printing heterogeneity constructs	• Use of UV light source • Bioink must be photocrosslinkable	• Vascularized constructs • Tissue models and cell-laden implants	[21–26]
	VBP	• Unprecedented printing speed (tens of seconds) • High cell viability (>90%) • Contactless printing • Ultra-low concentration bioinks • Possible to create geometrically complex constructs	• Centimeter-scale constructs • Relative low feature size resolution (30–500 μm) • Deep light penetration	• Complex constructs • Organoids • Scaffolds • Vascularized constructs	[49], [40, 50, 77, 85, 93], [80, 81]

DLP: digital-light processing. VBP: volumetric bioprinting. UV: ultraviolet.

the green body was subjected to thermal treatment of debinding steps (figure 10(A, ii)) and then was sintered to obtain a fully dense silica part (figure 10(A, iii)). The prints had unprecedented geometric freedom, low surface roughness, high breaking strength, and optical transparency in fused silica.

Kollep *et al* group volumetrically printed silicon oxycarbide ceramics successfully [73]. The printing procedure was divided into two steps (figure 10(B)). First, the 2D images of the printed object was projected at different angles onto the photosensitive polysiloxane preceramic resin (the resin used had a viscosity of 873°mPa s) and cured in the container. Then a ceramic was formed by pyrolysis at 1000 °C. The ceramic parts showed resistance in a high temperature for 20 s (figure 10(B, i)), and in HCl and KOH solutions for 1°h (figure 10(B, ii)). Figure 10(C) showed the different types of volumetrically printed glass constructs. Compared with traditional printing and pyrolysis, volumetric printing greatly improves fabrication efficiency and speeds up the model optimization cycle as well.

5. Outlook and future perspectives

In recent years, VBP has gained increasing attention due to its extremely fast printing speed, supportless printing modality (table 3) and high cell viability (table 4). Researchers are focusing on improving

Table 4. The cell types used in VBP.

Cell type	Cell concentration	Cell viability	Printing time	Model	Resolution	Biomaterials	Refs
C2C12	5×10^6 cells ml^{-1}	90% (14 d)	∼45 s	Screw	∼57 μm	SF	[49]
C2C12	5×10^6 cells ml^{-1}	250% (14 d)	∼45 s	Screw	∼45.9 μm	SS	[49]
ACPCs	1×10^7 cells ml^{-1}	>85% (7 d)	Seconds	Disc constructs	144.69 ± 13.55 μm	GelMA	[77]
Hepatic organoids	5×10^6 cells ml^{-1}	93.3 ±1.4% (10 d)	∼20 s	Sphere	41.5 ± 2.9 μm	GelMA	[50]
C2C12	1×10^6 cells ml^{-1}	90% (7 d)	Seconds	Spiral	∼200 μm	Gelatin–norbornene (Gel–NB)/PEG4SH	[40]
NHDF	1×10^6 cells ml^{-1}	90% (7 d)	∼10–11 s	Branch	∼200 μm	Gelatin–norbornene (Gel–NB)/PEG4SH	[40]
hMSC	3×10^6 cells ml^{-1}	>90%	<60 s	Vascularization	Micrometer-scale	GelMA	[78]
Human embryonic kidney 293	4×10^6 cells ml^{-1}	∼90%	Seconds	A construct with a core surrounded by four channels	∼100 μm	GelMA	[80]

C2C12: mouse myoblasts. ACPCs: articular chondroprogenitor cells. NHDF: normal human dermal fibroblasts. hMSCs: human mesenchymal stem cells. SF: silk fibroin. SS: silk sericin. GelMA: gelatin methacryloyl. PEG4SH: 4-Arm-PEG-thio.

printing resolution and fidelity of VBP through hardware and software aspects [44, 80]. Others are exploring and developing novel bioinks for VBP to expand its biomedical applications [83].

In future work, to meet complicated biomedical applications such as tissue engineering, regenerative medicine, *et al*, single material cannot satisfy these specific functions [98]. Therefore, multi-material and multi-cell VBP is in urgent need [13, 99]. The manufacture of organoids and large-scale tissue structures are hot topic applications [50, 51]. Additionally, *in situ* VBP might be an interesting direction [100].

Further, artificial intelligence (AI) assisted (bio)printing is a prospect direction. AI (especially machine learning) technique could be used to optimize printing parameters to compensate the cell-induced scattering effects, or to identify the optimized formulations of (bio)resins to improve printing resolution [82–84, 101]. Shaochen Chen *et al* group used machine learning to automatically generate the printer parameters to compensate scattering effects, which significantly improved the printing resolution [102, 103]. At last, it is predictable that VBP could facilitate fast medical device manufacturing such as microneedles, tooth, organ chips and flexible electronics [104, 105].

Data availability statement

No new data were created or analyzed in this study.

Acknowledgments

This work was supported by the Guangdong provincial basic and applied basic research fund provincial enterprise joint fund (Grant No. 2021A1515220174), and key scientific research project of university in Guangdong Province (Grant No. 2023KCXTD026). The authors have no other relevant affiliations or financial involvement with any organization or entity with a financial interest in or financial conflict with the subject matter or materials discussed in the manuscript apart from those disclosed.

Conflict of interest

All other authors declare they have no competing interests.

ORCID iD

Maobin Xie https://orcid.org/0000-0001-9082-4510

References

[1] Guillemot F, Mironov V and Nakamura M 2010 Bioprinting is coming of age: report from the International Conference on Bioprinting and Biofabrication in Bordeaux (3B'09) *Biofabrication* **2** 010201
[2] Groll J *et al* 2016 Biofabrication: reappraising the definition of an evolving field *Biofabrication* **8** 013001
[3] Li G, Wang J, Xu M, Zhang H, Tu C, Yang J, Chen X, Yao Q, Lan P and Xie M 2020 Engineered exosome for NIR-triggered drug delivery and superior synergistic chemo-phototherapy in a glioma model *Appl. Mater. Today* **20** 100723
[4] Quan H, Zhang T, Xu H, Luo S, Nie J and Zhu X 2020 Photo-curing 3D printing technique and its challenges *Bioact. Mater.* **5** 110–5
[5] Mazumder J 2015 Design for metallic additive manufacturing machine with capability for "certify as you build" *Proc. CIRP* **36** 187–92
[6] Suntornnond R, Ng W L, Huang X, Yeow C H E and Yeong W Y 2022 Improving printability of hydrogel-based bio-inks for thermal inkjet bioprinting applications via saponification and heat treatment processes *J. Mater. Chem.* B **10** 5989–6000

[7] Li X, Liu B, Pei B, Chen J, Zhou D, Peng J, Zhang X, Jia W and Xu T 2020 Inkjet bioprinting of biomaterials *Chem. Rev.* **120** 10793–833

[8] Ng W L, Xi H, Shkolnikov V, Goh G L, Suntornnond R and Yeong W Y 2021 Controlling droplet impact velocity and droplet volume: key factors to achieving high cell viability in sub-nanoliter droplet-based Bioprinting *Int. J. Bioprinting* **8** 424

[9] Xu T, Zhao W, Zhu J-M, Albanna M Z, Yoo J J and Atala A 2013 Complex heterogeneous tissue constructs containing multiple cell types prepared by inkjet printing technology *Biomaterials* **34** 130–9

[10] Ong C S *et al* 2017 Biomaterial-free three-dimensional bioprinting of cardiac tissue using human induced pluripotent stem cell derived cardiomyocytes *Sci. Rep.* **7** 4566

[11] Fu Z, Naghieh S, Xu C, Wang C, Sun W and Chen X 2021 Printability in extrusion bioprinting *Biofabrication* **13** 033001

[12] Zhang Y S, Haghiashtiani G, Hübscher T, Kelly D J, Lee J M, Lutolf M, McAlpine M C, Yeong W Y, Zenobi-Wong M and Malda J 2021 3D extrusion bioprinting *Nat. Rev. Methods Primers* **1** 75

[13] Ravanbakhsh H, Karamzadeh V, Bao G, Mongeau L, Juncker D and Zhang Y S 2021 Emerging technologies in multi-material bioprinting *Adv. Mater.* **33** 2104730

[14] Tavafoghi M *et al* 2021 Multimaterial bioprinting and combination of processing techniques towards the fabrication of biomimetic tissues and organs *Biofabrication* **13** 042002

[15] Ying G, Manríquez J, Wu D, Zhang J, Jiang N, Maharjan S, Hernández Medina D H and Zhang Y S 2020 An open-source handheld extruder loaded with pore-forming bioink for *in situ* wound dressing *Mater. Today Bio* **8** 100074

[16] Cheng R Y, Eylert G, Gariepy J-M, He S, Ahmad H, Gao Y, Priore S, Hakimi N, Jeschke M G and Günther A 2020 Handheld instrument for wound-conformal delivery of skin precursor sheets improves healing in full-thickness burns *Biofabrication* **12** 025002

[17] Duan B, Hockaday L A, Kang K H and Butcher J T 2013 3D bioprinting of heterogeneous aortic valve conduits with alginate/gelatin hydrogels *J. Biomed. Mater. Res.* **101A** 1255–64

[18] Chen M Y, Skewes J, Woodruff M A, Dasgupta P and Rukin N J 2020 Multi-colour extrusion fused deposition modelling: a low-cost 3D printing method for anatomical prostate cancer models *Sci. Rep.* **10** 10004

[19] Onoe H *et al* 2013 Metre-long cell-laden microfibres exhibit tissue morphologies and functions *Nat. Mater.* **12** 584–90

[20] de Beer M P, van der Laan H L, Cole M A, Whelan R J, Burns M A and Scott T F 2019 Rapid, continuous additive manufacturing by volumetric polymerization inhibition patterning *Sci. Adv.* **5** eaau8723

[21] Lee M, Rizzo R, Surman F and Zenobi-Wong M 2020 Guiding lights: tissue bioprinting using photoactivated materials *Chem. Rev.* **120** 10950–1027

[22] Levato R, Dudaryeva O, Garciamendez-Mijares C E, Kirkpatrick B E, Rizzo R, Schimelman J, Anseth K S, Chen S, Zenobi-Wong M and Zhang Y S 2023 Light-based vat-polymerization bioprinting *Nat. Rev. Methods Primers* **3** 47

[23] Ng W L, Lee J M, Zhou M, Chen Y-W, Lee K-X A, Yeong W Y and Shen Y-F 2020 Vat polymerization-based bioprinting—process, materials, applications and regulatory challenges *Biofabrication* **12** 022001

[24] Daly A C, Prendergast M E, Hughes A J and Burdick J A 2021 Bioprinting for the biologist *Cell* **184** 18–32

[25] Levato R 2021 High-resolution lithographic biofabrication of hydrogels with complex microchannels from low-temperature-soluble gelatin bioresins *Mater. Today Bio* **12** 100162

[26] Cheng J *et al* 2022 Centrifugal multimaterial 3D printing of multifunctional heterogeneous objects *Nat. Commun.* **13** 7931

[27] Tumbleston J R *et al* 2015 Additive manufacturing. Continuous liquid interface production of 3D objects *Science* **347** 1349–52

[28] Lipkowitz G *et al* 2022 Injection continuous liquid interface production of 3D objects *Sci. Adv.* **8** eabq3917

[29] Kelly B E, Bhattacharya I, Shusteff M, Panas R M, Taylor H K and Spadaccini C M 2017 pw Computed Axial Lithography (CAL):Toward Single Step 3D Printing of Arbitrary Geometries (arXiv:1705.05893)

[30] Cano-Vicent A, Tambuwala M M, Hassan S S, Barh D, Aljabali A A A, Birkett M, Arjunan A and Serrano-Aroca Á 2021 Fused deposition modelling: current status, methodology, applications and future prospects *Addit. Manuf.* **47** 102378

[31] Murphy C A, Lim K S and Woodfield T B F 2022 Next evolution in organ-scale biofabrication: bioresin design for rapid high-resolution vat polymerization *Adv. Mater.* **34** 2107759

[32] Zhou C *et al* 2021 Ferromagnetic soft catheter robots for minimally invasive bioprinting *Nat. Commun.* **12** 5072

[33] Heinrich M A *et al* 2019 Bioprinting: 3D Bioprinting: from Benches to Translational Applications (Small 23/2019) *Small* **15**

[34] Gu Z, Fu J, Lin H and He Y 2020 Development of 3D bioprinting: from printing methods to biomedical applications *Asian J. Pharmacol. Sci.* **15** 529–57

[35] Moroni L *et al* 2018 Biofabrication: a guide to technology and terminology *Trends Biotechnol.* **36** 384–402

[36] de Ruijter M, Ribeiro A, Dokter I, Castilho M and Malda J 2019 Simultaneous micropatterning of fibrous meshes and bioinks for the fabrication of living tissue constructs *Adv. Healthcare Mater.* **8** e1800418

[37] Bordini E A F, Cassiano F B, Bronze-Uhle E S, Alamo L, Hebling J, de Souza Costa C A and Soares D G 2022 Chitosan in association with osteogenic factors as a cell-homing platform for dentin regeneration: analysis in a pulp-in-a-chip model *Dent. Mater.* **38** 655–69

[38] Billiet T, Vandenhaute M, Schelfhout J, Van Vlierberghe S and Dubruel P 2012 A review of trends and limitations in hydrogel-rapid prototyping for tissue engineering *Biomaterials* **33** 6020–41

[39] Gudapati H, Dey M and Ozbolat I 2016 A comprehensive review on droplet-based bioprinting: past, present and future *Biomaterials* **102** 20–42

[40] Rizzo R, Ruetsche D, Liu H and Zenobi-Wong M 2021 Optimized photoclick (bio)resins for fast volumetric bioprinting *Adv. Mater.* **33** 2102900

[41] Shusteff M, Browar A E M, Kelly B E, Henriksson J, Weisgraber T H, Panas R M, Fang N X and Spadaccini C M 2017 One-step volumetric additive manufacturing of complex polymer structures *Sci. Adv.* **3** eaao5496

[42] Kelly B E, Bhattacharya I, Heidari H, Shusteff M, Spadaccini C M and Taylor H K 2019 Volumetric additive manufacturing via tomographic reconstruction *Science* **363** 1075–9

[43] Matlock A, Zhu J and Tian L 2023 Multiple-scattering simulator-trained neural network for intensity diffraction tomography *Opt. Express* **31** 4094–107

[44] Loterie D, Delrot P and Moser C 2020 High-resolution tomographic volumetric additive manufacturing *Nat. Commun.* **11** 852

[45] Regehly M, Garmshausen Y, Reuter M, König N F, Israel E, Kelly D P, Chou C-Y, Koch K, Asfari B and Hecht S 2020 Xolography for linear volumetric 3D printing *Nature* **588** 620–4

[46] Darkes-Burkey C and Shepherd R F 2020 High-resolution 3D printing in seconds *Nature* **588** 594–5

[47] Ehsan A A, Rahim M S and Woei H C 2019 Projection optics design for projection stereolithography 3D printer

2019 IEEE Regional Symp. on Micro and Nanoelectronics (RSM) (IEEE) pp 160–3
[48] Orth A *et al* 2022 Optical scattering tomography for volumetric additive manufacturing *Conf. on Lasers and Electro-Optics* (Optica Publishing Group) p ATh1D.3
[49] Xie M *et al* 2023 Volumetric additive manufacturing of pristine silk-based (bio)inks *Nat. Commun.* **14** 210
[50] Bernal P N *et al* 2022 Volumetric bioprinting of organoids and optically tuned hydrogels to build liver-like metabolic biofactories *Adv. Mater.* **34** e2110054
[51] Boniface A, Maître F, Madrid-Wolff J and Moser C 2023 Volumetric helical additive manufacturing *Light Adv. Manuf.* **4** 1
[52] Vock P, Soucek M, Daepp M and Kalender W A 1990 Lung: spiral volumetric CT with single-breath-hold technique *Radiology* **176** 864–7
[53] Goodarzi Hosseinabadi H, Dogan E, Miri A K and Ionov L 2022 Digital light processing bioprinting advances for microtissue models *ACS Biomater. Sci. Eng.* **8** 1381–95
[54] Ligon S C, Liska R, Stampfl J, Gurr M and Mülhaupt R 2017 Polymers for 3D printing and customized additive manufacturing *Chem. Rev.* **117** 10212–90
[55] Bagheri A and Jin J 2019 Photopolymerization in 3D printing *ACS Appl. Polym. Mater.* **1** 593–611
[56] Liu S, Borjigin T, Schmitt M, Morlet-Savary F, Xiao P and Lalevée J 2023 High-performance photoinitiating systems for LED-induced photopolymerization *Polymers* **15** 342
[57] Shi S, Croutxé-Barghorn C and Allonas X 2017 Photoinitiating systems for cationic photopolymerization: ongoing push toward long wavelengths and low light intensities *Prog. Polym. Sci.* **65** 1–41
[58] Ley C, Carre C, Ibrahim A and Allonas X 2017 Application of high performance photoinitiating systems for holographic grating recording (InTech) pp 375–404
[59] Swainson W K 1977 *Method, medium and apparatus for producing three-dimensional figure product* USA US4041476A
[60] Wang M *et al* 2022 Molecularly cleavable bioinks facilitate high-performance digital light processing-based bioprinting of functional volumetric soft tissues *Nat. Commun.* **13** 3317
[61] Axpe E, Orive G, Franze K and Appel E A 2020 Towards brain-tissue-like biomaterials *Nat. Commun.* **11** 3423
[62] Lian L *et al* 2022 Uniaxial and coaxial vertical embedded extrusion bioprinting *Adv. Healthcare Mater.* **11** 2102411
[63] Luo Z *et al* 2022 Vertical extrusion cryo(bio)printing for anisotropic tissue manufacturing *Adv. Mater.* **34** 2108931
[64] Anandakrishnan N *et al* 2021 Fast stereolithography printing of large-scale biocompatible hydrogel models *Adv. Healthcare Mater.* **10** 2002103
[65] Ge Q *et al* 2021 3D printing of highly stretchable hydrogel with diverse UV curable polymers *Sci. Adv.* **7** eaba4261
[66] Li W *et al* 2021 A smartphone-enabled portable digital light processing 3D printer *Adv. Mater.* **33** e2102153
[67] Wu D, Yu Y, Tan J, Huang L, Luo B, Lu L and Zhou C 2018 3D bioprinting of gellan gum and poly (ethylene glycol) diacrylate based hydrogels to produce human-scale constructs with high-fidelity *Mater. Des.* **160** 486–95
[68] Kim S H *et al* 2021 3D bioprinted silk fibroin hydrogels for tissue engineering *Nat. Protocols* **16** 5484–532
[69] De Santis M M *et al* 2021 Extracellular-matrix-reinforced bioinks for 3D bioprinting human tissue *Adv. Mater.* **33** e2005476
[70] Xue B, Zhang Y, Xu M, Wang C, Huang J, Zhang H, Meng S, Xie M, Tao A and Li X 2019 Curcumin-silk fibroin nanoparticles for enhanced anti-Candida albicans activity *in vitro* and *in vivo J. Biomed. Nanotechnol.* **15** 769–78
[71] Xie M, Li Y, Zhao Z, Chen A, Li J, Li Z, Li G and Lin X 2016 Development of silk fibroin-derived nanofibrous drug delivery system in supercritical CO_2 *Mater. Lett.* **167** 175–8
[72] Chawla S, Midha S, Sharma A and Ghosh S 2018 Silk-based bioinks for 3D bioprinting *Adv. Healthcare Mater.* **7** 1701204
[73] Kollep M *et al* 2022 Tomographic volumetric additive manufacturing of silicon oxycarbide ceramics *Adv. Eng. Mater.* **24** 2101345
[74] Wang B, Engay E, Stubbe P R, Moghaddam S Z, Thormann E, Almdal K, Islam A and Yang Y 2022 Stiffness control in dual color tomographic volumetric 3D printing *Nat. Commun.* **13** 367
[75] Martinez-Crespiera S, Ionescu E, Kleebe H J and Riedel R 2011 Pressureless synthesis of fully dense and crack-free SiOC bulk ceramics via photo-crosslinking and pyrolysis of a polysiloxane *J. Eur. Ceram. Soc.* **31** 913–9
[76] Kim J H, Kim K and Jin H-E 2022 Three-dimensional printing for oral pharmaceutical dosage forms *J. Pharm. Invest.* **52** 293–317
[77] Bernal P N, Delrot P, Loterie D, Li Y, Malda J, Moser C and Levato R 2019 Volumetric bioprinting of complex living-tissue constructs within seconds *Adv. Mater.* **31** 1904209
[78] Gehlen J, Qiu W, Schädli G N, Müller R and Qin X-H 2023 Tomographic volumetric bioprinting of heterocellular bone-like tissues in seconds *Acta Biomater.* **156** 49–60
[79] Toombs J T, Luitz M, Cook C C, Jenne S, Li C C, Rapp B E, Kotz-Helmer F and Taylor H K 2022 Volumetric additive manufacturing of silica glass with microscale computed axial lithography *Science* **376** 308–12
[80] Madrid-Wolff J, Boniface A, Loterie D, Delrot P and Moser C 2022 Controlling light in scattering materials for volumetric additive manufacturing *Adv. Sci.* **9** 2105144D
[81] Größbacher G *et al* 2023 Volumetric printing across melt electrowritten scaffolds fabricates multi-material living constructs with tunable architecture and mechanics *Adv. Mater.* **35** 2300756
[82] Bhattacharya I, Toombs J and Taylor H 2021 High fidelity volumetric additive manufacturing *Addit. Manuf.* **47** 102299
[83] Cook C C *et al* 2020 Highly tunable thiol-ene photoresins for volumetric additive manufacturing *Adv. Mater.* **32** 2003376
[84] Rackson C M, Champley K M, Toombs J T, Fong E J, Bansal V, Taylor H K, Shusteff M and McLeod R R 2021 Object-space optimization of tomographic reconstructions for additive manufacturing *Addit. Manuf.* **48** 102367
[85] Ribezzi D *et al* 2023 Shaping synthetic multicellular and complex multimaterial tissues via embedded extrusion-volumetric printing of microgels *Adv. Mater.* **35** 2301673
[86] Bertsch P, Diba M, Mooney D J and Leeuwenburgh S C G 2023 Self-healing injectable hydrogels for tissue regeneration *Chem. Rev.* **123** 834–73
[87] Ma J and Wu C 2022 Bioactive inorganic particles-based biomaterials for skin tissue engineering *Exploration* **2** 20210083
[88] Peng Y, Zhuang Y, Liu Y, Le H, Li D, Zhang M, Liu K, Zhang Y, Zuo J and Ding J 2023 Bioinspired gradient scaffolds for osteochondral tissue engineering *Exploration* **3** 20210043
[89] van Genderen A M *et al* 2020 Topographic guidance in melt-electrowritten tubular scaffolds enhances engineered kidney tubule performance *Front. Bioeng. Biotechnol.* **8** 617364
[90] Xie C, Gao Q, Wang P, Shao L, Yuan H, Fu J, Chen W and He Y 2019 Structure-induced cell growth by 3D printing of heterogeneous scaffolds with ultrafine fibers *Mater. Des.* **181** 108092
[91] Lim K S *et al* 2018 Bio-resin for high resolution lithography-based biofabrication of complex cell-laden constructs *Biofabrication* **10** 034101
[92] Zhu X, Li H, Huang L, Zhang M, Fan W and Cui L 2020 3D printing promotes the development of drugs *Biomed. Pharmacother.* **131** 110644
[93] Rodríguez-Pombo L, Xu X, Seijo-Rabina A, Ong J J, Alvarez-Lorenzo C, Rial C, Nieto D, Gaisford S, Basit A W

and Goyanes A 2022 Volumetric 3D printing for rapid production of medicines *Addit. Manuf.* **52** 102673
[94] Xu M, Li G, Zhang H, Chen X, Li Y, Yao Q and Xie M 2020 Sequential delivery of dual drugs with nanostructured lipid carriers for improving synergistic tumor treatment effect *Drug Deliv.* **27** 983–95
[95] Shen Y, Liang L, Zhang S, Huang D, Zhang J, Xu S, Liang C and Xu W 2018 Organelle-targeting surface-enhanced Raman scattering (SERS) nanosensors for subcellular pH sensing *Nanoscale* **10** 1622–30
[96] Kong F *et al* 2021 Targeting tumor lineage plasticity in hepatocellular carcinoma using an anti-CLDN6 antibody-drug conjugate *Sci. Transl. Med.* **13** eabb6282
[97] Zhang H, Huang L, Tan M, Zhao S, Liu H, Lu Z, Li J and Liang Z 2022 Overview of 3D-printed silica glass *Micromachines* **13** 81
[98] Liu Y, Xie M, Wang S, Zheng Q, Chen A and Deng Q 2013 Facile fabrication of high performances MTX nanocomposites with natural biomembrane bacterial nanoparticles using GP *Mater. Lett.* **100** 248–51
[99] Warner J, Soman P, Zhu W, Tom M and Chen S 2016 Design and 3D printing of hydrogel scaffolds with fractal geometries *ACS Biomater. Sci. Eng.* **2** 1763–70
[100] Hakimi N, Cheng R, Leng L, Sotoudehfar M, Ba P Q, Bakhtyar N, Amini-Nik S, Jeschke M G and Günther A 2018 Handheld skin printer: *in situ* formation of planar biomaterials and tissues *Lab Chip* **18** 1440–51
[101] Orth A, Sampson K L, Ting K, Boisvert J and Paquet C 2021 Correcting ray distortion in tomographic additive manufacturing *Opt. Express* **29** 11037
[102] Guan J, You S, Xiang Y, Schimelman J, Alido J, Ma X, Tang M and Chen S 2022 Compensating the cell-induced light scattering effect in light-based bioprinting using deep learning *Biofabrication* **14** 015011
[103] You S, Guan J, Alido J, Hwang H H, Yu R, Kwe L, Su H and Chen S 2020 Mitigating scattering effects in light-based three-dimensional printing using machine learning *J. Manuf. Sci. Eng.* **142** 081002
[104] Xu M *et al* 2023 Minimally invasive power sources for implantable electronics *Exploration* 20220106
[105] Leng F, Zheng M and Xu C 2021 3D-printed microneedles with open groove channels for liquid extraction *Exploration* **1** 20210109